A practical crosstalk attenuation method for separated wavefield imaging

Shaoping Lu, N.D. Whitmore, A.A. Valenciano, Nizar Chemingui and Grunde Rønholt, PGS*

Summary

Images of primaries and multiples can be contaminated by erroneous phantom images caused by the crosstalk of multiply scattered events. Using a causality property of the events in separated up- and down-going wavefields, we present a practical crosstalk prediction and attenuation method when imaging using surface reflected wavefields. Our method does not explicitly separate multiples of any specified order. Through both synthetic and field data examples, we show how the proposed method reliably predicts the crosstalk in separated wavefield imaging. Consequently, it provides higher quality images with balanced amplitudes and improved illumination.

Introduction

Primary reflections are generally the most useful source of signal for subsurface imaging. Multiple reflections are typically treated as noise to be suppressed in the data processing prior to the imaging stage. However, there has been an ever-increasing use of multiples as signal to be imaged, which can complement the primary image (Lu et al., 2011). Acquisition and processing methods can be used to separate the total wavefield into up- and down-going wavefields at the surface, which can be subsequently extrapolated into the subsurface and imaged. We define this process as Separated Wavefield IMaging (SWIM), in which the imaged multiples can improve the illumination of the subsurface, especially the shallow section (Lu et al., 2013). On the other hand, crosstalk due to different orders of surface scattering can contaminate both primary and multiple images. In order to provide the best overall image, this crosstalk needs to be attenuated.

Crosstalk is unavoidable, and can be coherent and difficult to remove directly within the imaging stage. One method for reducing crosstalk is least squares migration (Zhang et al., 2013, Wong et al., 2015, Tu and Herrmann 2015), in which the initially modeled data using the image with crosstalk will not match the recorded data. During iterations, both the residual in data domain and the crosstalk in the image domain are reduced. Another approach for removing crosstalk is full wavefield migration and inversion (Davydenko and Verschuur 2014). In either least squares or full wavefield imaging, several iterations of modeling and imaging are typically required to obtain an optimal image.

In the presentation, we describe a method of predicting and attenuating the crosstalk in both pre- and post-stack images based on the causality relationship of their position/time subject to their true reflection locations in the image domain. Through both synthetic and field data examples and under the framework of SWIM, we demonstrate that this method predicts and attenuates the crosstalk efficiently and thus can provide higher quality images with balanced amplitudes, improved illumination and attenuated crosstalk.

Method

We apply (one-way or two-way) wave equation migration for separated wavefield imaging, where the boundary data is the surface recorded wavefields. The separated up-going (P-UP) and down-going (P-DWN) wavefields consist of both primaries and surface reflections as follows:

$$\left.\begin{aligned} \text{P-UP} &= U_p + U_m^1 + U_m^2 + \ldots = U_m^0 + U_m^1 + U_m^2 + \ldots = \sum_i U_m^i \quad (1.1) \\ \text{P-DWN} &= D_p + D_m^1 + D_m^2 + \ldots = D_m^0 + D_m^1 + D_m^2 + \ldots = \sum_i D_m^i \quad (1.2) \end{aligned}\right\} \quad (1)$$

where U_m^0 and D_m^0 denote the primary wavefield in P-UP and P-DWN respectively; and U_m^i and D_m^i denote the i^{th} order multiple wavefield in P-UP and P-DWN respectively.

The fundamental concept of separated wavefield imaging is to utilize each receiver as a "virtual" source and propagate the P-DWN and P-UP waves as source and receiver wavefields respectively before correlating them using an appropriate imaging condition denoted by:

$$\left.\begin{aligned} \text{SWIM} &= \text{P-UP} \ * \ \text{P-DWN} \\ &= \sum_i \left(D_m^i * U_m^{i+1}\right) && \text{(2.1) Image} \\ &+ \sum_i \left[D_m^i * \left(U_m^{i+2} + U_m^{i+3} + \ldots\right)\right] && \text{(2.2) Causal crosstalk} \\ &+ \sum_i \left[D_m^i * \left(U_m^{i} + U_m^{i-1} + \ldots\right)\right] && \text{(2.3) Anti-causal crosstalk} \end{aligned}\right\} \quad (2)$$

Here, unfortunately, both the desired image and undesired crosstalk events are created in the raw image, where:

(1) The i^{th} order P-DWN wavefield D_m^i, and the $(i+1)^{th}$ order P-UP wavefield U_m^{i+1} are correlated to construct the desired image [Equation 2.1] .

(2) The i^{th} order P-DWN wavefield D_m^i, and the $(i+2)^{th}$ (and higher) orders of P-UP wavefield $U_m^{i+2} + U_m^{i+3} + \ldots$ are correlated to be the causal crosstalk [Equation 2.2], which are the events appear deeper than their true reflection positions [Figure 1C].

(3) The i^{th} order P-DWN wavefield D_m^i, and the i^{th} (and lower) orders of P-UP wavefield $U_m^i + U_m^{i-1} + \ldots$ are correlated to be the anti-causal crosstalk [Equation 2.3],

which are the events appear shallower than their true reflection positions [Figure 1D].

While a deconvolution imaging condition may reduce the remaining crosstalk in term 2.1 (Lu et al., 2015), crosstalk in the form of terms 2.2 and 2.3 are generally the strong coherent crosstalk which are not easy to attenuate in the imaging phase. Using the reversibility of the wavefield and matching the orders between the up-going and down-going wavefields, we have:

$$\left.\begin{aligned} \text{Anti-causal crosstalk} &= \sum_i \left[D_m^i * \left(U_m^i + U_m^{i-1} + \ldots\right)\right] \quad (3.1) \\ &= \sum_i \left[\left(D_m^i + D_m^{i+1} + \ldots\right) * U_m^i\right] \quad (3.2) \end{aligned}\right\} \quad (3)$$

Using this relationship and Equation 2, our proposed crosstalk prediction and attenuation scheme can be summarized as follows:

(1) The causal crosstalk prediction: we form an image in either pre- (e.g. angle) or post-stack domain using term 2.2 in Equation 2 by utilizing a source generated wavefield D_m^{-1} as the down-going wavefield and the multiple model P-UP wavefield $U_m^1 + U_m^2 + \ldots$ as the receiver wavefield [Figure 1E].

(2)The anti-causal crosstalk prediction: we form an image in either pre- (e.g. angle) or post-stack domain using term 3.2 in Equation 3 by utilizing all the P-DWN wavefield $D_m^0 + D_m^1 + \ldots$ as the down-going wavefield and the zeroth order P-UP wavefield U_m^0 as the receiver wavefield [Figure 1F].

(3) The crosstalk attenuation: in either pre- (e.g. angle) or post-stack where the crosstalk are predicted using step (1) and (2), apply appropriate subtraction method to the overall image found using Equation 2.

Examples

In the first example, our proposed method is applied to the Sigsbee2B synthetic example. The exact velocity model contains several large velocity contrasts at water bottom, along the salt body and at the deep horizontal mud horizon. The reflection energy resulted from these contrasts not only provide the desired strong reflectors in the image, but also generate undesired crosstalk contamination. In the raw SWIM image (after muting above the water bottom) presented in Figure 2A, we note the dominating casual crosstalk (blue arrows) appears to be a "peg-lag-image" of the true reflectors (appears as the conventional imaging of all the multiples using a point source). In fact, as demonstrated in the kinematic diagram in Figure 1C, this crosstalk is the result of the correlation between the first water bottom reflection in source wavefield and the second order multiples in receiver wavefield. On the other hand, the dominating anti-casual crosstalk (black arrows) has a shallower appearance compared to the position of the true reflector. As demonstrated in Figure 1D, this crosstalk is the result of the correlation between the water bottom reflections in source wavefield and all the primary events (e.g. the primary of the deep mud line) in the receiver wavefield.

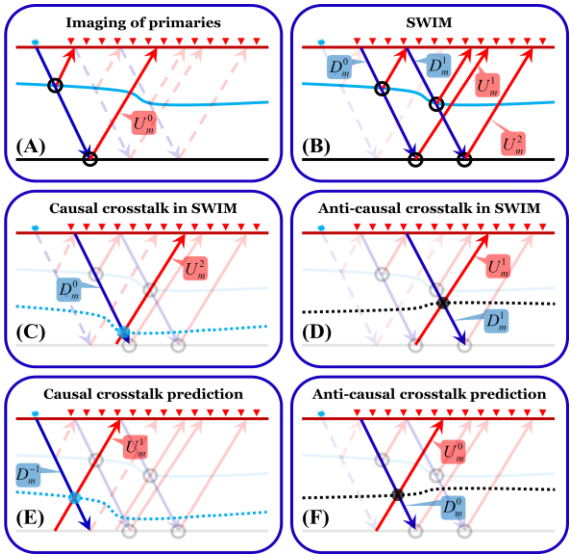

***Figure 1**, Raypath demonstration of formation of images using primaries (A) and SWIM (B) and the formation of the causal crosstalk in SWIM (C), anti-causal crosstalk in SWIM (D), causal crosstalk prediction for SWIM (E), and anti-causal crosstalk prediction for SWIM (F).*

Using our proposed crosstalk prediction scheme, the prediction of the causal crosstalk in Figure 2C is generated using an impulse wavelet and all the up-going multiples while the prediction of the anti-causal crosstalk in Figure 2B is generated using the entire down-going shot record and the up-going primaries. The predicted crosstalk provides an excellent match to the original crosstalk highlighted in Figure 2A and thus make the crosstalk attenuation using an image domain subtraction straightforward. Comparing to the raw SWIM image in Figure 2A, the image in Figure 2D after the crosstalk attenuation using the proposed method, has improved amplitude balance and enhanced resolution.

The second example performs crosstalk attenuation on a 2D field data example from Desoto Canyon Gulf of Mexico. The anti-causal crosstalk generated by the reflection energy from the water bottom is thus poorly affecting the shallow part of the raw SWIM image in Figure 3A and appears even across the water column section. Using our proposed method, the predicted anti-causal crosstalk in Figure 3B

and the causal crosstalk in Figure 3C provide an excellent kinematic matching to the crosstalk in Figure 3A. Comparing to the raw SWIM image in Figure 3A, the final image with improved resolution after the crosstalk attenuation in Figure 3D provides us a better understanding of the subsurface, especially in the shallow section where some of the crosstalk in Figure 3A may be misinterpreted as channels or faults.

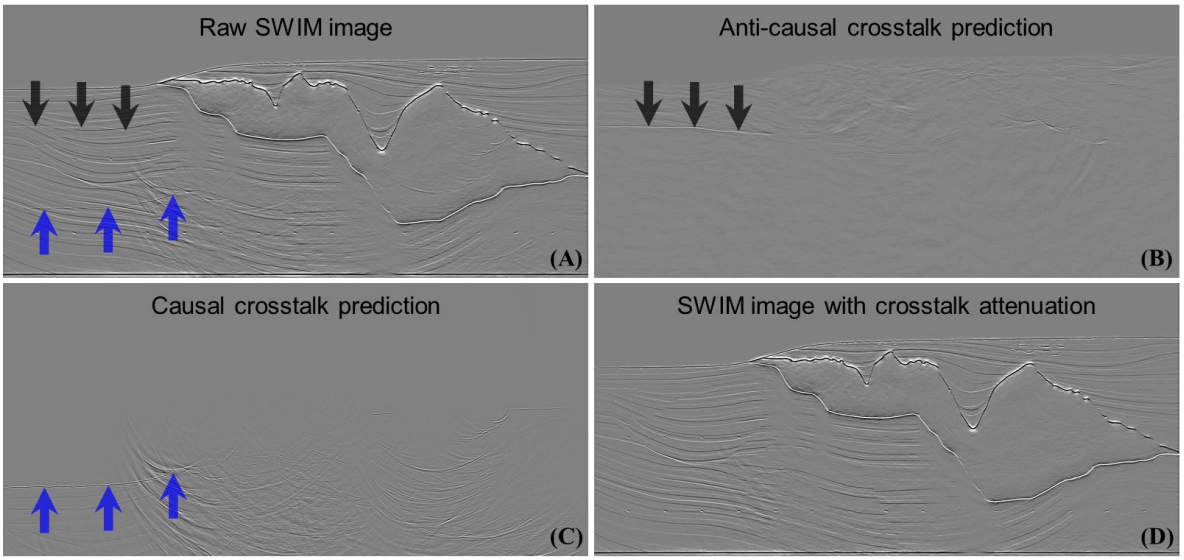

***Figure 2**, The Sigsbee2b synthetic example of raw SWIM image (A), anti-causal crosstalk prediction (B), causal crosstalk prediction (C), and the SWIM image after crosstalk attenuation (D).*

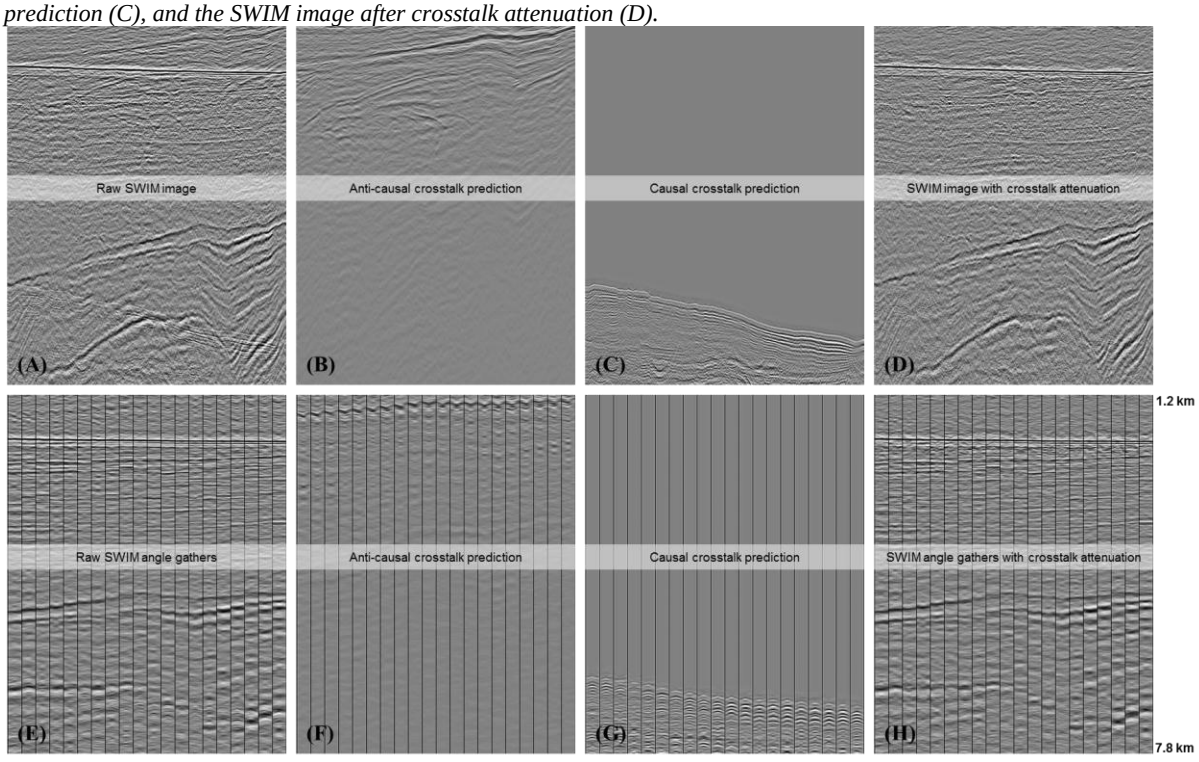

***Figure 3**, Zero angle images from Desoto Canyon 2D field data example (A-D), and angle gathers (F-H), -35 to +35 degree.*

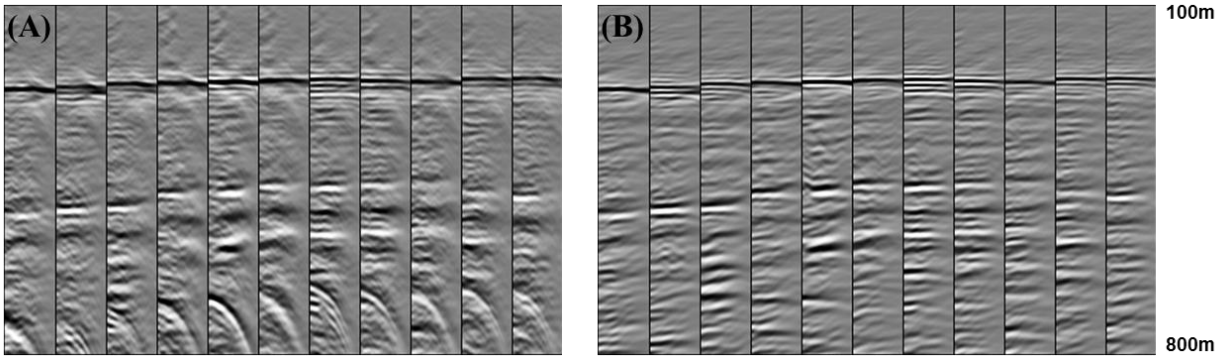

***Figure 4**, Raw SWIM angle gathers (A) versus SWIM angle gathers after crosstalk attenuation (B), zero to 45 degree, from Barents Sea 3D field data example.*

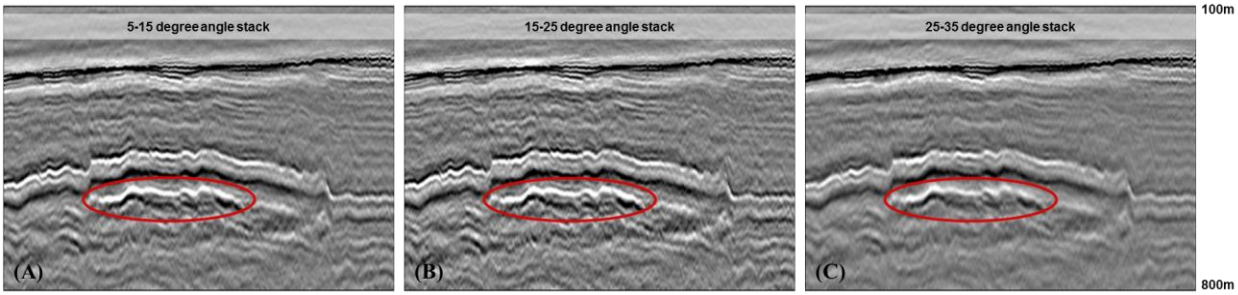

***Figure 5**, Stacked images from SWIM angle gathers over 5 to 15 degree (A), 15 to 25 degree (B), and 25 to 35 degree from Barents Sea 3D field data example. The target area (red circle) shows clear AVA behaviors.*

We further verify the quality of our crosstalk attenuation by replacing the imaging condition for generating Figures 3A-D with an imaging condition outputting subsurface angle gathers. The corresponding results are shown in Figures 3E-H. In these figures, we note that the true subsurface reflection points have no move-out while the causal and anti-causal crosstalk have a positive and negative move-out respectively. Assuming the migration velocity is optimal, the crosstalk events are migrated using incorrect wave propagation paths, which result in incorrect depths and move-out in accord with an incorrect velocity field. The subsurface angle gathers after the crosstalk attenuation in Figure 3H confirm the improvement in the image quality using our proposed method.

We have also applied the method to a 3D field data example from Barents Sea. The raw SWIM angle gathers consists of both causal and anti-causal crosstalk [Figure 4A]. We image the crosstalk in the angle domain and remove them to create clean angle gathers [Figure 4B]. The SWIM angle gathers can be used for angle dependent attribute analysis (Rønholt et. al., 2015). In Figure 5, we show stacked images from different angle ranges: 5-15 degree in 5A, 15-25 degree in 5B, and 25-35 degree in 5C. We are able to observe clear AVA anomalies in the angle stacked images.

Conclusions

Separated wavefield imaging enables us to create high-resolution images from using the surface reflected wavefield for migration. The technology has been involving issues of crosstalk. We discussed the origin of the strong causal and anti-causal crosstalk in SWIM. We have demonstrated the method of predicting and attenuating the crosstalk in both pre- and post-stack domain via migration. Through both synthetic and field data examples and under the framework of SWIM, we demonstrate that this method predicts and attenuates the crosstalk efficiently and thus can provide higher quality images with balanced amplitudes, improved illumination and attenuated crosstalk.

Acknowledgements

We thank PGS for permission to publish the work and the data.

EDITED REFERENCES

Note: This reference list is a copyedited version of the reference list submitted by the author. Reference lists for the 2016 SEG Technical Program Expanded Abstracts have been copyedited so that references provided with the online metadata for each paper will achieve a high degree of linking to cited sources that appear on the Web.

REFERENCES

Davydenko, M., and D. J. Verschuur, 2014, Full wavefield migration in three dimensions: 84th Annual International Meeting, SEG, Expanded Abstracts, 3935–3940, http://dx.doi.org/10.1190/segam2014-1079.1.

Lu, S., N. D. Whitmore, A. A. Valenciano, and N. Chemingui, 2011, Imaging of primaries and multiples with 3D SEAM synthetic: 81st Annual International Meeting, SEG, Expanded Abstracts, 3217–3221, http://dx.doi.org/10.1190/1.3627864.

Lu, S., N. D. Whitmore, H. LeGleut, and A. Long, 2013, 3D high-resolution imaging using separated wavefields: 75th Annual International Conference and Exhibition, EAGE, Extended Abstracts, paper no. 68902.

Lu, S., N. D. Whitmore, A. A. Valenciano, and N. Chemingui, 2015, Separated-wavefield imaging using primary and multiple energy: The Leading Edge, **34**, 770–778, http://dx.doi.org/10.1190/tle34070770.1.

Rønholt, G., Ø. Korsmo, S. Naumann, S. Marinets, E. Brenne, and M. F. Abbasi, 2015, Complete wavefield imaging for lithology and fluid prediction in the Barents Sea: 85th Annual International Meeting, SEG, Expanded Abstracts, 4070–4074, http://dx.doi.org/10.1190/segam2015-5869968.1.

Tu, N., and F. Herrmann, 2015, Fast least-squares imaging with surface-related multiples: Application to a North Sea data set: The Leading Edge, **34**, 788–794, http://dx.doi.org/10.1190/tle34070788.1.

Wong, M., B. L. Biondi, and S. Ronen, 2015, Imaging with primaries and free-surface multiples by joint least-squares reverse time migration: Geophysics, **80**, no. 6, S223–S235, http://dx.doi.org/10.1190/geo2015-0093.1.

Zhang, Y., L. Duan, and Y. Xie, 2013, A stable and practical implementation of least-squares reverse time migration: 83rd Annual International Meeting, SEG, Expanded Abstracts, 3716–3720, http://dx.doi.org/10.1190/segam2013-0577.1.